AIP | The Journal of Chemical Physics

Structure and phase behavior of polymer loaded non-ionic and anionic microemulsions

Andreas Weber and Bernd Stühn

Citation: The Journal of Chemical Physics **144**, 144903 (2016); doi: 10.1063/1.4945610
View online: http://dx.doi.org/10.1063/1.4945610
View Table of Contents: http://scitation.aip.org/content/aip/journal/jcp/144/14?ver=pdfcov
Published by the AIP Publishing

Structure and phase behavior of polymer loaded non-ionic and anionic microemulsions

Andreas Weber[a] and Bernd Stühn
Institute for Condensed Matter Physics, Technische Universität Darmstadt, Darmstadt, Germany

(Received 30 November 2015; accepted 25 March 2016; published online 12 April 2016)

We investigate the structure and phase behavior of $C_{12}E_4$ based reverse water in octane microemulsions with small angle x-ray scattering and small angle neutron scattering experiments to explore the phase diagram of the droplet structure. In the regime of stable droplets, these droplets are loaded with the hydrophilic polymer polyethyleneoxide (M_W = 1500 g/mol) and compared with microemulsions based on the anionic surfactant AOT. In the small angle neutron scattering experiments, we use shell contrast to focus on the surfactant shell and its variation with addition of polymer. We observe, as predicted by indirect measurements such as dielectric spectroscopy, that the polymer interacts differently with a nonionic or an anionic surfactant shell: In the former case the addition of polymer does not seem to affect the surfactant shell. In the latter case, the obtained scattering data show that the anionic surfactant layer is strongly influenced leading to a higher polydispersity which may be attributed to a floppier surfactant shell. *Published by AIP Publishing.* [http://dx.doi.org/10.1063/1.4945610]

I. INTRODUCTION

Microemulsions are ternary mixtures of a polar and a nonpolar liquid stabilized by a surfactant. Macroscopically they are transparent and isotropic. Microscopically, microemulsions form nanostructures on the scale of a few nanometers where polar and nonpolar phases are separated by a surfactant layer. A variety of different microstructures has been observed, depending on composition of the system and external parameters such as temperature and pressure. In this publication, we focus on a reverse micelle structure in which nanoscopic water spheres are dissolved in an oil matrix by a surfactant.

Microemulsions have a vast range of applications. Drug delivery,[1] oil recovery,[2] and the usage of microemulsion micelles as reactor for chemical reactions[3] are some prominent examples.

Microemulsions with spherical structures may serve as systems for the investigation of the behavior of polymers at curved surfactant layers and in a situation of soft confinement. It is known that the addition of polymers to microemulsions may change their structural and dynamical behavior, depending on the investigated microemulsion system and polymer. It has been observed that addition of a hydrophobic polymer to a microemulsion system composed by the same amount of water and oil induces the one phase regions of microemulsions to shrink and shifts the phase transition line to higher temperatures.[4]

From measurements with dielectric spectroscopy it is known that the polymer polyethyleneoxide (PEO) interacts differently with non-ionic and anionic surfactant shells. Conductivity measurements show that addition of PEO to a water/AOT/octane microemulsions with sufficiently big micelles shifts the percolation temperature to higher temperatures. At the percolation temperature, an infinite cluster of microemulsion droplets forms leading to an immense increase of the electric conductivity of the system.[5] The temperature shift increases with polymer concentration and saturates at a certain concentration. Assuming an attractive force between polymer and surfactant, this saturation is due to a complete adsorption of the polymer to surfactant layer.[6] In similar measurement on a microemulsion system containing $C_{12}E_5$, this effect has not been detected: The addition of polymer does not affect the percolation behavior and, thus, the bending rigidity of the surfactant shell, leading to the conclusion that a steric repulsion between polymer and surfactant dominates.[7] Theoretical studies of the interaction between polymer and surfactants confirm these findings.[8]

Addition of an amphiphilic diblock copolymer provokes the so called boosting effect, which means that a lower surfactant concentration is needed for mixing polar and nonpolar liquid.[9,10] On the other hand, adding hydrophilic and hydrophobic homopolymer the efficiency of the surfactant decreases (anti-boosting effect).[11] It has been shown that triblock copolymers with two hydrophobic blocks at the ends of the molecule and a hydrophilic midblock deform water in oil-microemulsion droplets,[12] while oil in water-microemulsions maintain their spherical structure. They may form a transient network of droplets connected by the triblock copolymers.[13]

Apart from the chemical properties of the polymers, knowledge about the location of the polymer in a microemulsion phase seems to be crucial to understand the effects of the polymer on the structure and dynamics of the microemulsion. The objective of this work is to directly compare the influence of low molecular weight PEO on the structure of droplet phase microemulsions with anionic or non-ionic surfactants, respectively. Furthermore we try to examine by means of scattering experiments, where the polymer chains are located inside water droplets. For the AOT

[a]Electronic mail: andreas.weber@fkp.physik.tu-darmstadt.de

based microemulsions, a number of studies of scattering data is present. Temperature, droplet size, and concentration were varied in numerous studies.[14–21] An important conclusion of these studies is that a stable droplet phase is present in a wide range of the phase diagram and for temperatures from the supercooled state up to an upper phase boundary covering up to 70 K. C_iE_j based microemulsion have been investigated extensively.[22,23] As the curvature of this surfactant type is controlled strongly by temperature, one can generate oil in water or water in oil structures by varying temperature.[24] The phase behavior of different C_iE_j based microemulsion systems generally displays the same features but phase boundaries are shifted depending on the composition of the system.[25] For this reason, it is important to determine a phase diagram to identify the stable areas before proceeding with loading of polymer into the droplet structure.

This paper is organised as follows: The first part is dedicated to the determination of the phase diagram of inverse $C_{12}E_4$ based microemulsions in the droplet phase by small angle x-ray scattering (SAXS). We investigate the stability of the droplet phase regarding the mixing parameters W, Φ and variations of the temperature. We show that there is a dependency of the droplet volume fraction Φ on the water core radii which will be explained in terms of the monomeric solubility of the surfactant in the excess phase of the system. Having once determined a phase diagram, we investigate the influence of PEO on the phase behavior of the system. In a final step, we perform small angle neutron scattering (SANS) measurements on $C_{12}E_4$ based microemulsions as well as AOT based microemulsions in shell contrast experiments. This gives a sharp contrast between the components of the system and thus scattering data which provide precise structural parameters of the investigated system. We show that the influence of PEO on the non-ionic microemulsion is small but for the anionic system, there is a significant effect on the polydispersity of the droplets.

II. EXPERIMENTAL

A. Samples

To define the composition of a water in oil microemulsion, we use the molar water to surfactant ratio,

$$W = \frac{N_{\text{Water}}}{N_{\text{Surfactant}}}, \tag{1}$$

and the volume fraction of microemulsion droplets in the sample,

$$\Phi = \frac{V_{\text{Droplet}}}{V_{\text{Total}}} = \frac{V_{\text{Water}} + V_{\text{Surfactant}}}{V_{\text{Water}} + V_{\text{Surfactant}} + V_{\text{Oil}}}. \tag{2}$$

Microemulsion samples with Φ and W were prepared as follows: First, a water/polymer stock solution was prepared with the wanted polymer concentration c. A certain amount of surfactant was put into a vessel and weighed. The exact amount of water/polymer solution and octane was calculated and added to the vessel. The sample was shaken until it was transparent. Before each measurement, samples were stored for several hours to achieve thermodynamic equilibrium.

The amount of polymer in the microemulsion is defined by the concentration of polymer in water c. A more intuitive concept is the average number of polymer chains per microemulsion droplet,

$$z = \frac{N_{\text{P}}}{N_{\text{D}}} = \frac{c}{1 + c/\rho_{\text{P}}} \frac{N_A}{M_{\text{P}}} \frac{4}{3} \pi r_C^3, \tag{3}$$

where N_{P}, ρ_{P}, and M_{P} are the total number of polymer chains in the sample, the bulk polymer density, and its molar mass, respectively. The total number of microemulsion droplets with water core radius r_C in the sample is N_{D}.

The components of the microemulsions for the X-ray scattering study were water (Millipore Direct-Q3 ultrapure water system, $\sigma_r = 5.5 \cdot 10^{-8}$ S cm^{-1}), $C_{12}E_4$, octane, and PEO (obtained from Sigma-Aldrich, used as received).

For the neutron scattering study, we prepared samples with shell contrast. Thus, water (99% purity, Sigma-Aldrich) and octane (98% purity, Euriso-Top) were deuterated, but the surfactants $C_{12}E_4$ and AOT (Sigma-Aldrich) were not. All components were used as received.

PEO had a molecular weight $M_n = 1500$ g/mol. The radius of gyration of the polymer under θ-conditions was estimated to be 14 Å.[26] This estimation was confirmed by SANS measurements.[27]

Figure 1 shows the investigated samples for exploring the phase behavior of the microemulsion in a Gibbs phase plot. Table I summarizes the samples investigated in the SANS study. Here, values for W have been chosen such that droplet radii of both sample systems, prepared with non-ionic or anionic surfactant, are comparable.

B. Small angle scattering

The structure of the microemulsions was investigated by small angle scattering experiments using neutrons or

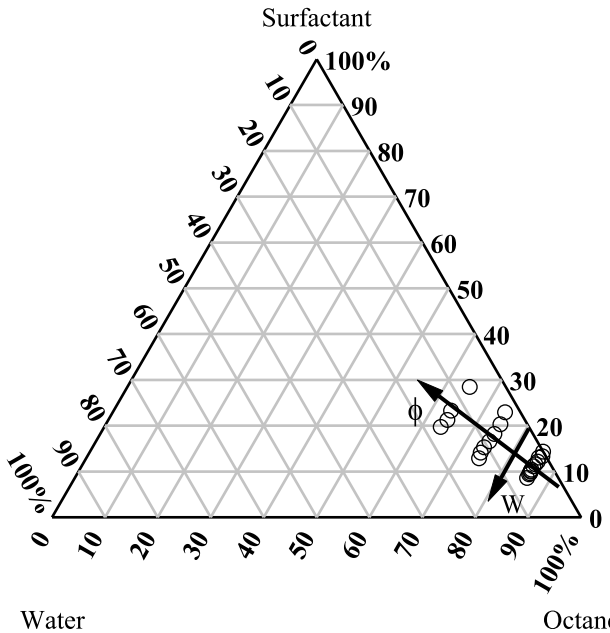

FIG. 1. Gibbs plot of $C_{12}E_4$ samples investigated by small angle x-ray scattering.

TABLE I. Samples investigated in the neutron scattering study. z is the number of polymer chains per droplet calculated with the effective water core radius, while z' is number of polymer chains per droplet calculated assuming an unaltered water core radius determined with Equation (8). c is the concentration of polymer in water in g/l. The volume fraction of microemulsion droplets was $\Phi = 0.11$ for all samples.

$C_{12}E_4$				AOT			
W	z	z'	c	W	z	z'	c
10.7	0	0	0	23.3	0	0	0
11.0	1.3	1.3	17.8	23.5	1.2	1.2	20.0
11.3	2.9	2.7	35.9	23.4	2.3	2.4	40.3
8.1	0	0	0	16.2	0	0	0
8.1	1.5	1.3	42.4	16.4	1.3	1.2	57.3
				16.4	2.4	2.4	115.5
17.0	0	0	0	33.9	0	0	0
15.8	1.2	0.9	4.6	33.3	0.9	0.8	4.6
17.1	2.8	2.4	9.7	33.7	2.0	1.7	9.7

X-rays. The phase diagram of the $C_{12}E_4$ based water-in-octane microemulsion was explored by preparing various samples and performing small angle X-ray scattering in a range of temperatures. Further experiments focussing on the effect of polymer in microemulsions were done with small angle neutron scattering. The experimental setups will now be introduced briefly.

1. Small angle X-ray scattering

SAXS measurements were performed with two experimental setups both using a wavelength of $\lambda = 1.54$ Å. One is a point-collimated setup with a 2-D multiwire detector. More details of the instrument are given elsewhere.[21] The second setup is a Kratky compact camera with a slit-collimated beam. The x-ray beam is monochromized by a Ni-filter. The scattered intensity is detected by a scintillation counter (sample-detector distance 20 cm). Temperature control of the sample cell in both instruments is better than $\Delta T = \pm 1$ K. Microemulsion samples are filled into sealed glass capillaries which fit into the sample cells. The obtained intensity patterns from the Kratky camera are desmeared using standard algorithms.[28]

2. Small angle neutron scattering

SANS measurements on samples with $W \approx 11$, $W \approx 8$ ($C_{12}E_4$ microemulsions) and $W \approx 23$, $W \approx 16$ (AOT microemulsions) were performed at the KWS-1[29] instrument operated by Jülich Centre for Neutron Science (JCNS) and FRM II at the Heinz Maier-Leibnitz Zentrum (MLZ), Garching, Germany. Wavelength of the neutrons was 4.5 Å. Detector distances were set to 1.5 m, 8 m, and 20 m, thus covering a q-Range from 0.003 Å^{-1} to 0.4 Å^{-1}. Samples with $W \approx 17$ ($C_{12}E_4$ microemulsions) and $W \approx 33$ (AOT microemulsions) were investigated at D11 of the Institute Laue-Langevin (ILL) in Grenoble with $\lambda = 4.6$ Å and detector distances 1.2 m and 8 m, covering a q-Range from 0.01 Å^{-1} to 0.67 Å^{-1}. Collimation at both setups were set to 8 m and 20 m for detector distances 1.2-8 m and 20 m, respectively. At both setups, samples were measured in *Hellma* cuvettes with 1 mm thickness. Acquired raw data were normalised and reduced using JCNS and ILL standard procedures, respectively.

III. ANALYSIS OF THE SCATTERING PROFILES

Small angle scattering experiments probe the scattering length density distribution of the sample and allow the investigation of the structure of the sample. The resulting intensity of a scattering experiment in dependence on the scattering vector, $\vec{q}$ with $q = \frac{4\pi}{\lambda}\sin\theta$ (in the case of elastic scattering) is

$$I(\vec{q}) \propto S(\vec{q})|F(\vec{q})|^2, \tag{4}$$

where the form factor F is the fourier transform of the scattering length density distribution $\varrho(\vec{r})$ of a single particle,[30]

$$F(\vec{q}) = \int \varrho(\vec{r}) \exp(i\vec{q}\vec{r}) d\vec{r}. \tag{5}$$

For that, scattering experiments are sensitive on the contrast in the scattering length density distribution, $\varrho_{droplet} - \varrho_{matrix}$ in the case of droplets dispersed in a matrix.

We expect spherical droplets in the samples and therefore model the intensity patterns with a appropriate form factor.[31] Radial polydispersity was taken into account with a Schultz-Zimm distribution.[32] This polydispersity may be caused by a size distribution of droplet radii or shape fluctuations of the surfactant shell and will be discussed later in Sec. IV. A constant background was added to the model data.

X-ray scattering experiments are sensitive to the electron density ρ_{el} of the investigated system, which is connected to the scattering length density via $\varrho = \rho_{el} r_e$ with the classical electron radius $r_e = 2.818 \cdot 10^{-15}$ m. As there is nearly no contrast between the water core of the droplet and the head groups of the $C_{12}E_4$ surfactant molecules in the non-ionic sample system, we used the simple model of spheres dissolved in a matrix for the form factor. Fixing the electron densities and the corresponding scattering length densities ($\varrho_{\text{droplet}} = 9.46 \cdot 10^{-6}$ Å^{-2}, $\varrho_{\text{matrix}} = 7.05 \cdot 10^{-6}$ Å^{-2}), droplet radius and polydispersity were varied when fitting the model to the data.

For modelling the obtained SANS data, we used a core-shell model: Because of the fact that both water and oil matrix were deuterated and the surfactant shell not, there is a huge contrast between water core, surfactant shell and surrounding oil matrix. Figure 2 sketches the scattering length density profile for a microemulsion droplet investigated by SANS. In addition, in the case of the anionic AOT system, the contrast between surfactant head and tail is resolvable, so that we had to take into account two shells. To decrease the number of parameters in the SANS fitting process we applied the following restrictions (see also Table II): In both sample systems, ionic and non-ionic microemulsions, the scattering length density of the matrix ϱ_O and surfactant shell ϱ_S were kept fixed to the theoretical values.

Assuming that a part of a surfactant molecule with volume v_S and area a_s at the water-oil interface may penetrate or dissolve in the water core, the scattering length density of the core is

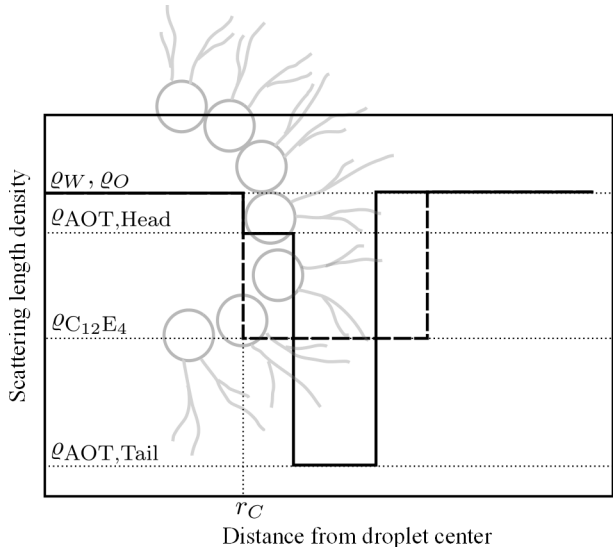

FIG. 2. SANS: Scattering length density profile for the $C_{12}E_4$ microemulsion (continuous line) and the AOT microemulsion (dashed line).

$$\varrho_{Core} = \varrho_{D_2O} - \frac{N v_S}{V}\left(\varrho_{D_2O} - \varrho_S\right), \tag{6}$$

with the volume V of a droplet and the number $N = 4\pi r_C^2/a_S$ of surfactant molecules per droplet. Thus, the scattering length density ϱ_{core} was allowed to vary according to

$$\varrho_{Core} = \varrho_{D_2O} - \frac{K}{r_C}\left(\varrho_{D_2O} - \varrho_S\right) \tag{7}$$

to take the penetration of surfactant into the water core into account. The parameter $K = 3v_S/a_S$ was fitted globally for all samples without polymer and was kept fixed when polymer was added. It roughly describes the penetration depth of the hydrophilic surfactant part into the water core. This will be discussed in detail in Sec. IV. The water core radius r_C and its relative polydispersity σ_C were fitted for each sample. The shell thickness of the water/AOT droplets in the ionic systems was subdivided into two parts with fixed lengths. The shell thickness of the water/$C_{12}E_4$ droplets in the non-ionic systems

TABLE II. SANS model parameters.

	Non-ionic system	Anionic system
ϱ_{D_2O}	$6.37 \cdot 10^{-6}$ Å^{-2} (fixed)	
ϱ_O	$6.42 \cdot 10^{-6}$ Å^{-2} (fixed)	
ϱ_S	$7.69 \cdot 10^{-8}$ Å^{-2} (fixed)	Head $5.65 \cdot 10^{-6}$ Å^{-2} (fixed) Tail $-3.8 \cdot 10^{-7}$ Å^{-2} (fixed)[35]
ϱ_C	Fitted according to Eq. (7)	
d_S	15.8 Å (Fitted globally with $z = 0$ samples)	Head 2 Å (fixed) Tail 8 Å (fixed)
r_C	Fitted	
σ	Fitted	
r_{HS}	Fixed to $r_{HS} = r_C + d_S$	
η	Fitted	

was fitted globally for all samples without polymer and kept fixed when polymer was added.

The structure factor S given in Eq. (4) describes the interference due to correlations between separated droplets in the sample. In our case, we model these interactions with a simple hard sphere model,[33] where the effective interaction distance $2r_{HS} = 2(r_C + d_S)$ was linked to the total size of one droplet, where d_S is the total shell thickness. The hard sphere volume fraction η was allowed to vary in the fitting process.

Table II summarizes the model parameters. Finally, to account for the experimental resolution, the model function was convoluted with a Gaussian resolution function with a standard deviation $\sigma = \frac{q}{2\sqrt{2\ln 2}}\frac{\Delta\lambda}{\lambda}$. Here $\frac{\Delta\lambda}{\lambda}$ is the wavelength spread of the experimental setups[34] (D11: $\frac{\Delta\lambda}{\lambda} = 0.09$, KWS-1: $\frac{\Delta\lambda}{\lambda} = 0.1$).

SAXS measurements allow to investigate the polar radius (water core radius + hydrophilic head of surfactant molecule) of $C_{12}E_4$ microemulsions. In the case of AOT based microemulsion, it is possible to determine water core radii and surfactant shell thickness because of the pronounced contrast between the components. SANS measurements allow us to determine these properties also for the $C_{12}E_4$ system as we prepared the system in shell contrast condition. Furthermore, they enable us to investigate polydispersity and the penetration depth of the hydrophilic surfactant part into the water core K.

IV. RESULTS

We first discuss the data of the polymer-free microemulsion systems for determining the phase diagram of the investigated system. After that we focus on the SANS study, the description of the scattering data and the effects on adding polymer chains to the microemulsion droplets.

A. Phase behavior of water/$C_{12}E_4$/octane microemulsions in the droplet state

Figure 3 shows SAXS patterns of water/$C_{12}E_4$/octane microemulsions for different W at constant $\Phi = 0.11$. The data show typical features for a droplet phase. From intermediate to high q, an interference shoulder due to intraparticle scattering is visible. When W is increased this shoulder systematically shifts to lower q implying an increase in droplet size. Nevertheless, this interference is not well pronounced since the ethylene oxide units of $C_{12}E_4$ have a very low contrast to water, the alkane units additionally have a low contrast to octane (see Section III) and we suppose that droplet radii are rather polydisperse. Because of the lack of contrast, we describe the data with a simple model applying a spherical form factor. For this reason, the radii of $C_{12}E_4$/water droplets obtained by SAXS are the polar radii. The full line in Figure 3 is a exemplary fit with the discussed model. The scattering data are well described aside from the smeared-out side maximum at $q \approx 0.1$ Å. This taint is due to the neglect of the surfactant shell in the SAXS model. The obtained polydispersities for all samples are quite high ($\sigma_C \approx 0.25$–0.30) but hard to interpret as both, the little pronounced interference and the tiny side maximum, are affected by this parameter. As the droplet volume fraction is low ($\Phi = 0.11$), there is a just small

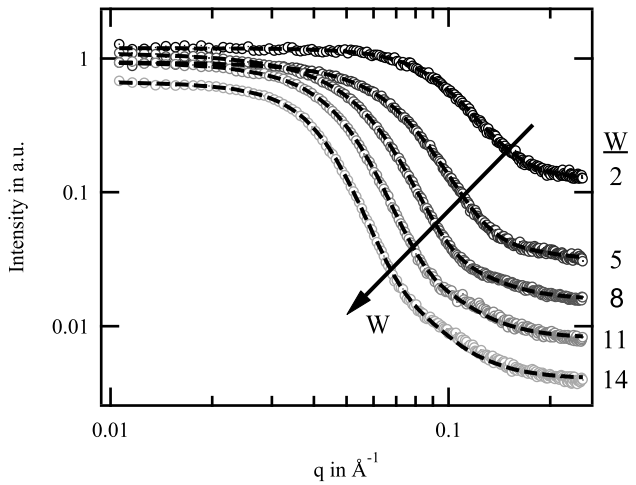

FIG. 3. SAXS profiles for the water/$C_{12}E_4$/octane microemulsion at constant $\Phi = 0.11$. The arrow shows the direction of increasing W. For clarity, the different curves have been shifted vertically. Dashed lines: Fits according to the model explained in Section III.

contribution of the structure factor on the intensity which will not be discussed further. Instead, we focus now on the radii of the microemulsion droplets.

1. Droplet radii dependence on composition of the microemulsion

The obtained droplet radii versus the molar water to surfactant ratio are shown in Figure 4. The droplet radii grow as W grows. This behavior is expected, as the volume of the water core is simply assumed to be $W n_a v_W$, where $v_W = 30$ Å^3 is the volume of one water molecule. The surface of such a water droplet of radius r_C is assumed to be fully covered by N surfactant molecules, each of them requiring an area A at the polar/non-polar interface. From these geometric considerations, the droplet radius is simply calculated by[36]

$$r_C(W) = \frac{3}{A} v_W W. \tag{8}$$

This relation is found to be nicely followed for microemulsions based on the surfactant AOT.[37]

Because of the low contrast between water core and polar head group of the surfactant, one has to add here the length of the head group, leading to a non-zero value for $W = 0$. In fact, one notes that for each Φ, there is a nearly linear relationship between W and the droplet radius. However, the slope obviously varies with Φ. Apparently with increasing Φ, a fraction of surfactant molecules does not contribute to the formation of water droplets. To explain this observation, one has to take into account the unimeric solubility of the surfactant molecule in the oil matrix.[38] Assuming that N_U surfactant molecules are dissolved in the oil matrix, one has to correct the water to surfactant ratio for the surfactant molecules that participate in forming the droplet structure,

$$W_i = \frac{N_{\text{Water}}}{N_{\text{Surfactant}} - N_U} = W\left(1 - \gamma_U \frac{1-\Phi}{\Phi}\left(W \frac{M_W}{\rho_W}\frac{\rho_O}{M_T} + \frac{\rho_O}{\rho_S}\right)\right)^{-1}. \tag{9}$$

M_i and ρ_i are the molar masses and mass densities of the components, and $\gamma_U = m_U/m_O$ is the ratio between the total mass of unimeric dissolved surfactant and the mass of the oil matrix. Applying this correction by fitting globally the γ_U value to the obtained droplet radii, they collapse on one linear relationship $r(W_i)$ as shown in Figure 5. From the slope we obtain $A = (53.7 \pm 1.9)$ Å^2 as surface per surfactant molecule at the water interface. The y-intercept is (12.4 ± 0.8) Å and matches perfectly to the length of the ethyleneoxide head of the surfactant molecule. The ratio of unimeric dissolved surfactant in oil was found to be $\gamma_U = 0.045 \pm 0.004$.

2. Temperature dependence of phase behavior

In comparison to microemulsions based on other surfactants, it is known that C_iE_j based microemulsions form an inverse droplet structure only in a small temperature region.[39] In order to investigate the temperature dependence of the phase diagram of the microemulsions, we measured the scattering of the samples varying temperature between 22 °C and 40 °C with $\Delta T = 2$ K steps. We find the SAXS profiles to be well described by the above explained model of spherical

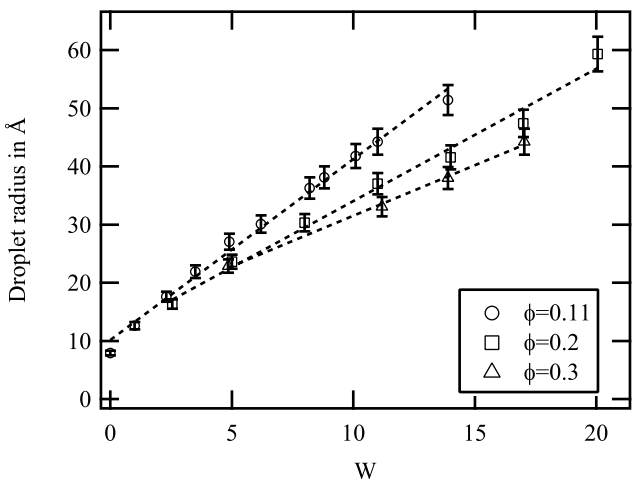

FIG. 4. Droplet radii obtained for the water/$C_{12}E_4$/octane microemulsion at varying W and Φ.

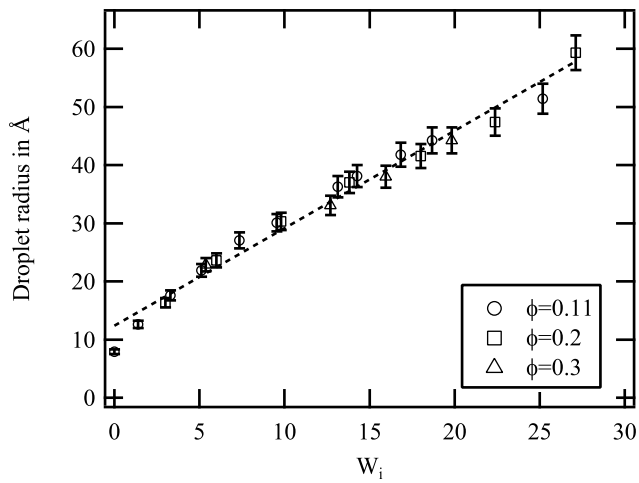

FIG. 5. Droplet radii obtained for the water/$C_{12}E_4$/octane microemulsion versus corrected water to surfactant ratio W_i (Eq. (9)).

particles and droplet radii have been extracted from the model. Figure 6 shows the obtained droplet radii for all investigated temperatures and W-series at fixed volume fraction of droplets $\Phi = 0.2$. One observes that for each W, the core radius is approximately constant up to a critical temperature. Above this temperature, droplet radii decrease and converge to one decaying curve for all W. This is the phase boundary between the one-phase microemulsion system and a two phase system consisting of a droplet phase and an excess phase of water. At this emulsification failure boundary, the maximum droplet radius which is obtainable minimizes the bending energy of the surfactant shell. The average mean curvature $H = 1/r$ of this optimum radius is proportional to the spontaneous curvature of the surfactant shell.[40] It depends linearly on temperature,[41] $H \propto T - T_C$. At T_C the surfactant has no preferred curvature and attempts to form flat or bicontinuous structures. Hence, the divergence of r is described by $r \propto (T - T_C)^{-1}$ and, fitting this equation to the phase border (see black line in Figure 6), we get $T_C = (13.5 \pm 0.8)\,°C$.

Having identified the regions of a stable droplet microemulsion, we study now the effect of adding PEO to the system. As a first step, the previously discussed SAXS experiments were repeated with similar mixtures but with an amount of polymer added such that, assuming that the polymer is located inside the droplets, there is on average $z = 1$ polymer chain in one droplet. The scattering patterns confirmed that the systems consisted of droplets again and there was no notable change in the radii of the droplets. Addition of polymer leads to a slight shift of the emulsification failure boundary as can been seen in Figure 6 (dashed line). The critical temperature is decreased to $T_C = (12.2 \pm 0.4)\,°C$. This means that at fixed temperature, the added polymer leads to a slight increase of the preferred curvature of the surfactant.

B. Small angle neutron scattering: Polymer-free microemulsions

To investigate the effect of PEO on microemulsion droplets and surfactant shell in detail, a comparative small angle neutron scattering study of an AOT based and a $C_{12}E_4$ based microemulsion was performed. Neutron scattering allows measurements with shell contrast meaning that only the surfactant shell (and later on the PEO chains) is protonated and the water inside the droplets and the surrounding oil matrix is deuterated (see Figure 2). Figure 7 shows the SANS patterns for both microemulsion systems. Due to the rather sharp contrast between d-water, surfactant and d-octane there are pronounced interferences in the intermediate q range. On these data, we applied the model discussed in the previous chapter resulting in a very good description of all data. This allows for an analysis of the obtained model parameters. Figure 8 shows all radii depending on W obtained by SANS in comparison with those obtained by SAXS at the same Φ. The linearity of the radii in W confirms again our expectations of a phase with isolated spherical droplets dispersed in a matrix. All obtained radii from the SANS measurements of the $C_{12}E_4$ system are systematically smaller than the radii obtained by SAXS measurements. Due to the different scattering contrasts SANS is sensitive to the water core while SAXS measurements

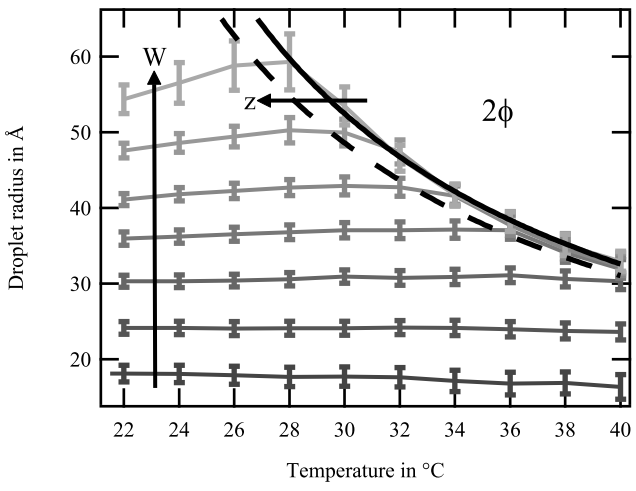

FIG. 6. Droplet radii obtained for the water/$C_{12}E_4$/octane microemulsion versus temperature. The dashed line indicates the shift of the phase transition upon addition of PEO to the microemulsion.

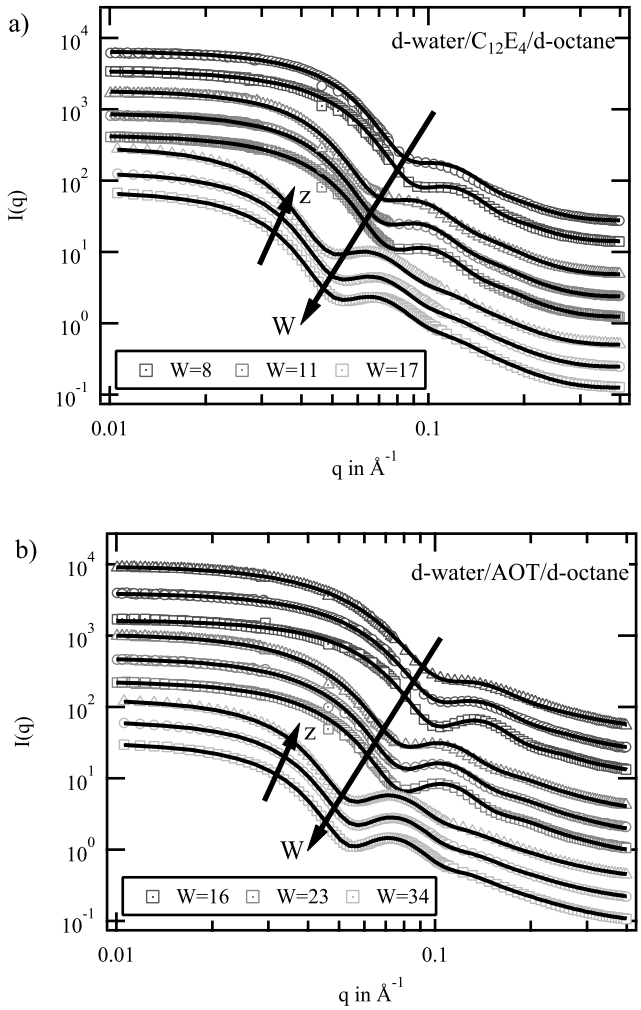

FIG. 7. Neutron scattering patterns for the (a) $C_{12}E_4$ and (b) AOT microemulsion system. For each W three or two different polymer loadings z are shown. The arrows show the direction of increasing W or z. The lines show the model function discussed. The measurements have been done at $T = 25\,°C$ (AOT: $W = 16$ and $W = 23$, $C_{12}E_4$: $W = 8$ and $W = 11$) and $T = 20\,°C$ (AOT: $W = 34$, $C_{12}E_4$: $W = 17$). For clarity, the different curves have been shifted vertically.

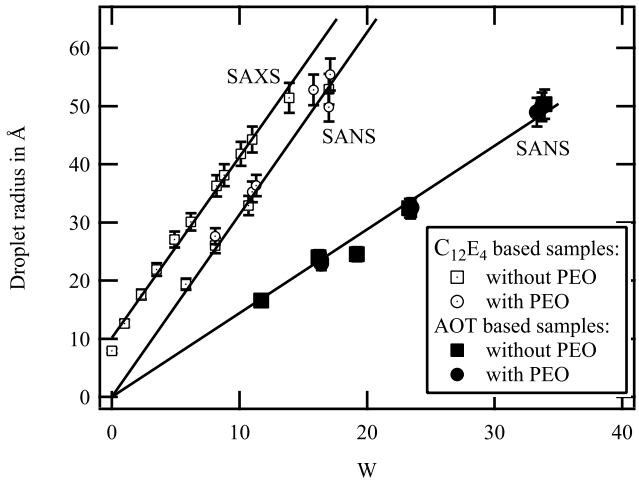

FIG. 8. Droplet radii vs. molecular water-to-surfactant ratio W for $\Phi = 0.11$. The shown radii measured by SAXS have been obtained at the temperature of the emulsification boundary, radii measured by SANS have been obtained at the respective temperature of the experiment.

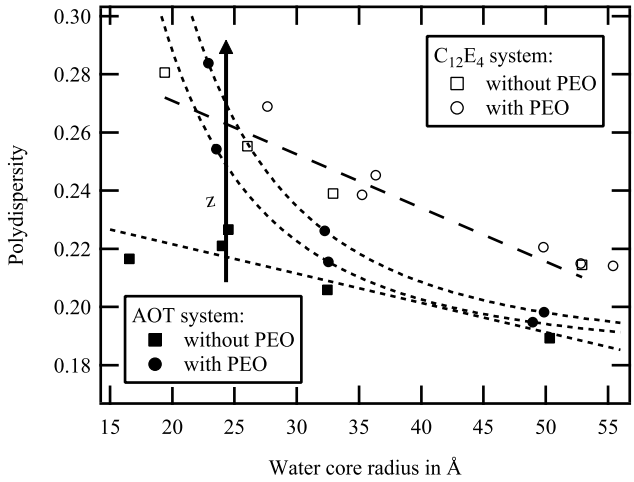

FIG. 9. Polydispersity of the microemulsion droplets obtained by SANS.

see the polar core of the microemulsion droplets. The shift between the obtained radii is about 10 Å and in the order of the size of the polar head of the surfactant.

The model presented in the previous chapter includes the parameter K which describes a variation of the scattering length density of the droplet core. This may be caused by the volume v_S of the surfactant which is fully dissolved in the water core. From the global fit of Eq. (7) we obtained for the AOT microemulsions $K = (1.17 \pm 0.01)$ Å. This corresponds to a volume $v_S = 25$ Å^3 which alters the scattering length density of the water core per AOT molecule. A sphere of that volume has a radius of $r = 1.8$ Å and is of the size of the dissolved sodium ions.

For the $C_{12}E_4$ microemulsions the variation in the scattering length density of the water core is well described by the variation of the parameter K but less intuitively to interpret than in the AOT case. In Eq. (7) $\frac{K}{3}$ might be interpreted as penetration depth leading to a more diffuse step in the scattering length density distribution (see Fig. 2) and thus leading to a decrease in the average scattering length density of the droplet core. With $K = (7.72 \pm 0.02)$ Å we find a penetration volume $v_S = (137.8 \pm 4.9)$ Å^3. The total volume of polyethyleneoxide head group (E_4) can be estimated with its density and molar mass. As it is around 240 Å^3, we conclude that approximately 60% of the EO head group is completely dissolved in the water core.

The high contrast between shell and the other microemulsion components allows us a detailed fitting of polydispersity and to interpret the polydispersity of the droplets. Mainly there are two different effects that contribute to the polydispersity of microemulsions: First, the radii of the droplets in a system are distributed around a mean droplet radius and the width of this distribution in mainly determined by the interfacial tension at the water and oil interface loaded with surfactant.[42] Second, the surfactant shell of a microemulsion droplet undergoes thermal shape fluctuations because of the floppiness of the shell.[43] Both effects combine to the measured polydispersity and cannot be distinguished as SANS measures a time averaged scattering profile of the sample.

Figure 9 shows the polydispersity of the microemulsion droplets in dependency on the droplet radii. In both microemulsion systems polydispersity grows when decreasing the droplet size. In the AOT system without polymer there is only a slight dependency of the polydispersity on the water core radii as it varies between 0.19 and 0.22 for droplet radii of 50 Å and 16.5 Å, respectively. In contrast, the polydispersity of the $C_{12}E_4$ microemulsion droplets increases from 0.21 to 0.28 in the same range of droplet radii.

This can be understood with the behavior of microemulsions at the above discussed emulsification failure boundary which separates the one phase microemulsion and a two phase system. Close to the emulsification boundary droplets behave like ideal spheres.[44,45] As the droplet volume is fixed by the composition of the microemulsion system, decreasing temperature from the emulsification boundary into the one phase region to the experimental temperature of the SANS measurements leads to a difference between the droplet radius and the preferred radius of the droplet. Thus, droplets become more flexible[46] and more polydisperse. Due to the molecular geometry of AOT, this effect is not as pronounced as in the $C_{12}E_4$ microemulsion system where the surfactant curvature is strongly temperature dependent. As all SANS measurements have been done at constant temperature, one can see from Figure 6 that bigger droplets were closer to the emulsification failure boundary and, thus, less polydisperse than small droplets for which the one phase region is more extended to higher temperatures.

C. Small angle neutron scattering: Polymer-loaded microemulsions

Now the effect of adding polymer to the microemulsion system will be investigated. We compare microemulsion with no polymer and microemulsion with $z \approx 1$ or $z \approx 2$. As before, SANS patterns were described by the above mentioned model, but taking into account a calculated, slightly lower core scattering length density because of the hydrophilic polymer

inside the droplets. Again, the model describes the data well and we conclude that the use of a mean value for z is justified.

The obtained core radii are displayed together with the core radii of the polymer-free system in Figure 8. One can see that the addition of polymer does nearly not affect the obtained water core radii of both microemulsion systems. With the number of EO-monomers in a polymer chain $N_{EO} = 34$ and the number of water molecules per droplet $V_C/v_w \approx \frac{4}{3}\pi r_C^3/30\ \text{Å}^3$, one can estimate that for the smallest droplets and the highest polymer concentration investigated the expected change in the droplet radius is not larger than 5% and, for that, the influence on the scattering patterns should be small.

However there is a clear impact of polymer addition on polydispersity in the case of AOT. Figure 9 compares polydispersity for both microemulsion systems with and without polymer. The polydispersity of the investigated $C_{12}E_4$ microemulsion droplets is not affected upon polymer addition. Contrary to this, the polydispersity of the AOT polymer-loaded microemulsions increases. This effect is more pronounced for smaller droplets and higher z while for the biggest droplets investigated there is almost no influence on the polydispersity.

This different behavior is due to different types of interaction between polymer and surfactant shell. In the case of the non-ionic surfactant $C_{12}E_4$ the polymer is sterically repulsed by the surfactant shell[7] and, thus, does not change significantly the properties of the droplets. This is also supported by the already discussed phase diagram of polymer-free and polymer-loaded microemulsion that revealed that the emulsification failure boundary is only slightly shifted to lower temperatures upon polymer addition (see Figure 6).

In anionic microemulsions PEO is expected to adsorb to the surfactant layer and thus to influence the layer properties.[7] If this is the case, then the droplet properties should change systematically with the relative coverage of the inner surfactant surface Ξ by the polymer. Assuming all chain segments to be in contact with the surfactant/water interface, the fraction of surface coverage is

$$\Xi = \frac{a N_{EO} z}{4\pi r_C^2} \tag{10}$$

where $a = 39\ \text{Å}^2$ is the area of an EO-monomer at an interface.[12] Figure 10 shows the polydispersity of the polymer-loaded AOT microemulsions dependent on the surface coverage. The linear variation of polydispersity with Ξ is nicely followed by our data as demonstrated in the figure and supports strongly the expectation of adsorbing polymer chains.

The polydispersity of the droplets is connected to the $l = 0$ mode of the shell fluctuation[47] which is a kind of "breathing" movement of the surfactant shell. Its amplitude depends inversely on the elastic constants of the surfactant layer. For this reason a higher polydispersity may be related to a lower bending rigidity. Thus, addition of PEO to the AOT microemulsions seems to cause a floppier surfactant shell. This picture is in agreement with a recent work by *Kuttich et al.*[48] who investigated the shell dynamics of AOT microemulsion with neutron spin echo spectroscopy. They observed that for droplets with $W < 25$ addition of PEO leads to slower shell dynamics and, thus, to a lower bending rigidity.

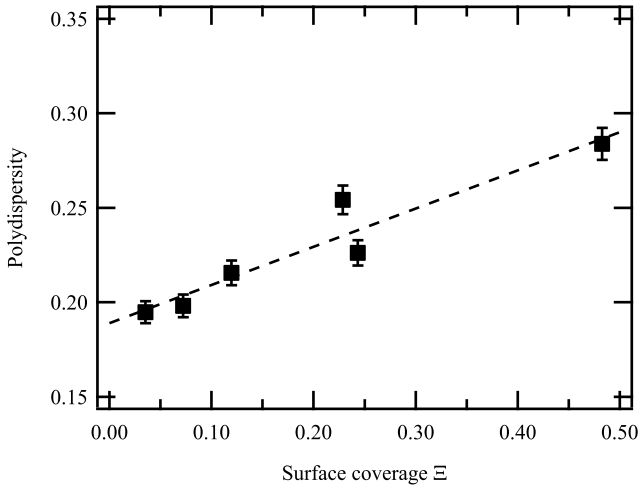

FIG. 10. Polydispersity vs. coverage of the inner surfactant surface with polymer for all AOT based microemulsions.

For bigger droplets one observes that polymer addition causes a shift of the percolation temperatures of the microemulsion system. This shift was related to an increase of the bending rigidity.[6] In agreement with this finding, polydispersity of our AOT microemulsions with $W \approx 34$ does vary only slightly with polymer addition.

V. CONCLUSION

We presented a detailed small angle scattering study on reverse microemulsions based on the surfactant $C_{12}E_4$. On the basis of this data we constructed a phase diagram of the droplet phase consisting of reversed water micelles in an oil matrix. We do indeed find the well known linear relationship between droplet radius and molecular water to surfactant ratio independent of droplet density if the unimeric solubility of surfactant in the oil matrix is considered.

The emulsification failure boundary between a one phase system and a two phase system consisting of a droplet and an excess phase is well described with a phase line on which the droplet radii behave like $r_C \propto (T - T_C)^{-1}$.

Addition of the hydrophilic polymer PEO to the $C_{12}E_4$ system does not change its properties significantly. Structure and phase behavior remain unchanged, although there is a slight shift of the temperature of the emulsification failure boundary.

A small angle neutron scattering study on this system and a comparable AOT system prepared in shell contrast provides insight into the question where the polymer is located in the microemulsion droplets. In the AOT system we observed an influence of the polymer on the polydispersity of the droplets and we conclude that the polymer adsorbs to the surfactant shell. In contrast of that, polydispersity of the $C_{12}E_4$ does not change. We therefore conclude that in the case of the non-ionic surfactant based system the polymer is located as an isolated chain inside the water droplet.

ACKNOWLEDGMENTS

Financial support by the "Deutsche Forschungsgemeinschaft" DFG through Project Nos. STU 191/4-1 and

STU 191/6-1 (DFG Forschergruppe 1583) is thankfully acknowledged. We thank the "Forschungs-Neutronenquelle Heinz Maier-Leibnitz" (FRM II) and the "Institut Laue-Langevin" (ILL) for beam time.

[1]M. Jayne Lawrence and G. D. Rees, "Microemulsion-based media as novel drug delivery systems," Adv. Drug Delivery Rev. **45**(1), 89–121 (2000).
[2]J. W. Jawitz, M. D. Annable, P. S. C. Rao, and R. Dean Rhue, "Field implementation of a winsor type i surfactant/alcohol mixture for *in situ* solubilization of a complex LNAPL as a single-phase microemulsion," Environ. Sci. Technol. **32**(4), 523–530 (1998).
[3]M. Magno, D. G. Angelescu, and C. Stubenrauch, "Phase diagrams of nonionic microemulsions containing reducing agents and metal salts as bases for the synthesis of bimetallic nanoparticles," Colloids Surf., A **348**(13), 116–123 (2009).
[4]A. C. John, H. Uchiyama, K. Nakamura, and H. Kunieda, "Phase behavior of a water/nonionic surfactant/oil ternary system in the presence of polymer oil," J. Colloid Interface Sci. **186**(2), 294–299 (1997).
[5]S. Bhattacharya, J. P. Stokes, M. W. Kim, and J. S. Huang, "Percolation in an oil-continuous microemulsion," Phys. Rev. Lett. **55**, 1884–1887 (1985).
[6]R. Wipf, S. Jaksch, and B. Stühn, "Dynamics in water-aot-n-decane microemulsions with poly(ethylene glycol) probed by dielectric spectroscopy," Colloid Polym. Sci. **288**(5), 589–601 (2010).
[7]W. Meier, "Poly(oxyethylene) adsorption in water/oil microemulsions: A conductivity study," Langmuir **12**(5), 1188–1192 (1996).
[8]P. G. De Gennes, "Interactions between polymers and surfactants," J. Phys. Chem. **94**(22), 8407–8413 (1990).
[9]B. Jakobs, T. Sottmann, R. Strey, J. Allgaier, and D. Richter, "Amphiphilic block copolymers as efficiency boosters for microemulsions," Langmuir **15**(20), 6707–6711 (1999).
[10]T. Sottmann, "Solubilization efficiency boosting by amphiphilic block copolymers in microemulsions," Curr. Opin. Colloid Interface Sci. **7**(1-2), 57–65 (2002).
[11]D. Byelov, H. Frielinghaus, O. Holderer, J. Allgaier, and D. Richter, "Microemulsion efficiency boosting and the complementary effect. 1. Structural properties," Langmuir **20**(24), 10433–10443 (2004).
[12]M. Müller, B. Stühn, K. Busse, and J. Kressler, "Modification of a reverse microemulsion with a fluorinated triblock copolymer," J. Colloid Interface Sci. **335**(2), 228–233 (2009).
[13]M. Schwab and B. Sthn, "Relaxation phenomena and development of structure in a physically crosslinked nonionic microemulsion studied by photon correlation spectroscopy and small angle x-ray scattering," J. Chem. Phys. **112**(14), 6461–6471 (2000).
[14]W. Jahn and R. Strey, "Microstructure of microemulsions by freeze fracture electron microscopy," J. Phys. Chem. **92**(8), 2294–2301 (1988).
[15]S. Nave, J. Eastoe, R. K. Heenan, D. Steytler, and I. Grillo, "What is so special about aerosol-ot? 2. Microemulsion systems," Langmuir **16**(23), 8741–8748 (2000).
[16]S.-H. Chen, S.-L. Chang, and R. Strey, "Structural evolution within the one-phase region of a three-component microemulsion system: Water-n-decane-sodium-bis-ethylhexylsulfosuccinate (AOT)," J. Chem. Phys. **93**(3), 1907–1918 (1990).
[17]S. H. Chen, J. Rouch, F. Sciortino, and P. Tartaglia, "Static and dynamic properties of water-in-oil microemulsions near the critical and percolation points," J. Phys.: Condens. Matter **6**(50), 10855 (1994).
[18]L. Arleth and J. S. Pedersen, "Droplet polydispersity and shape fluctuations in AOT [bis(2-ethylhexyl)sulfosuccinate sodium salt] microemulsions studied by contrast variation small-angle neutron scattering," Phys. Rev. E **63**, 061406 (2001).
[19]S. Lipgens, D. Schbel, L. Schlicht, J.-H. Spilgies, G. Ilgenfritz, J. Eastoe, and R. K. Heenan, "Percolation in nonionic water-in-oil-microemulsion systems: A small angle neutron scattering study," Langmuir **14**(5), 1041–1049 (1998).
[20]M. Nagao, H. Seto, M. Shibayama, and N. L. Yamada, "Small-angle neutron scattering study of droplet density dependence of the water-in-oil droplet structure in a ternary microemulsion," J. Appl. Crystallogr. **36**(3, Part 1), 602–606 (2003).
[21]M. Kraska, M. Domschke, and B. Stuhn, "Concentration induced ordering of microemulsion droplets in bulk and near the liquid-air interface," Soft Matter **9**, 3488–3496 (2013).
[22]R. Strey, "Microemulsion microstructure and interfacial curvature," Colloid Polym. Sci. **272**(8), 1005–1019 (1994).
[23]M. Gradzielski, D. Langevin, and B. Farago, "Experimental investigation of the structure of nonionic microemulsions and their relation to the bending elasticity of the amphiphilic film," Phys. Rev. E **53**, 3900–3919 (1996).
[24]F. Sicoli and D. Langevin, "Shape fluctuations of microemulsion droplets," J. Phys. Chem. **99**(40), 14819–14823 (1995).
[25]R. Aveyard, B. P. Binks, and P. D. I. Fletcher, "Interfacial tensions and aggregate structure in pentaethylene glycol monododecyl ether/oil/water microemulsion systems," Langmuir **5**(5), 1210–1217 (1989).
[26]L. J. Fetters, D. J. Lohse, and R. H. Colby, "Chain dimensions and entanglement spacings," in *Physical Properties of Polymers Handbook*, edited by J. E. Mark (Springer, New York, 2007), pp. 447–454.
[27]See supplementary material at http://dx.doi.org/10.1063/1.4945610 for SANS patterns and analysis of PEO in water.
[28]G. R. Strobl, "A new method of evaluating slit-smeared small-angle X-ray scattering data," Acta Crystallogr., Sect. A **26**(3), 367–375 (1970).
[29]H. M.-L. Zentrum, "KWS-1: Small-angle scattering diffractometer," J. Large-Scale Res. Facil. **1**, A28 (2015).
[30]A. Guinier, *X-Ray Diffraction In Crystals, Imperfect Crystals and Amorphous Bodies* (Dover Publications, 1987).
[31]S. H. Chen, "Small angle neutron scattering studies of the structure and interaction in micellar and microemulsion systems," Annu. Rev. Phys. Chem. **37**(1), 351–399 (1986).
[32]M. Kotlarchyk, R. B. Stephens, and J. S. Huang, "Study of Schultz distribution to model polydispersity of microemulsion droplets," J. Phys. Chem. **92**(6), 1533–1538 (1988).
[33]N. W. Ashcroft and J. Lekner, "Structure and resistivity of liquid metals," Phys. Rev. **145**, 83–90 (1966).
[34]I. Grillo, "Small-angle neutron scattering and applications in soft condensed matter," in *Soft Matter Characterization*, edited by R. Borsali and R. Pecora (Springer, Netherlands, 2008), pp. 723–782.
[35]R. Wipf, M. Kraska, T. Spehr, J. Nieberle, H. Frey, and B. Stühn, "Interaction between a water-in-oil microemulsion and a linear-dendritic poly(propylene oxide)-polyglycerol block copolymer," Soft Matter **7**, 10879–10888 (2011).
[36]M. A. Van Dijk, J. G. H. Joosten, Y. K. Levine, and D. Bedeaux, "Dielectric study of temperature-dependent aerosol ot/water/isooctane microemulsion structure," J. Phys. Chem. **93**(6), 2506–2512 (1989).
[37]M. Domschke, M. Kraska, R. Feile, and B. Stühn, "AOT microemulsions: Droplet size and clustering in the temperature range between the supercooled state and the upper phase boundary," Soft Matter **9**, 11503–11512 (2013).
[38]M. Kahlweit, R. Strey, and G. Busse, "Microemulsions: A qualitative thermodynamic approach," J. Phys. Chem. **94**(10), 3881–3894 (1990).
[39]S. Schrödle, R. Buchner, and W. Kunz, "Percolating microemulsions of nonionic surfactants probed by dielectric spectroscopy," ChemPhysChem **6**(6), 1051–1055 (2005).
[40]S. A. Safran, "Saddle-splay modulus and the stability of spherical microemulsions," Phys. Rev. A **43**, 2903–2904 (1991).
[41]R. Strey, "Phase behavior and interfacial curvature in water-oil-surfactant systems," Curr. Opin. Colloid Interface Sci. **1**(3), 402–410 (1996).
[42]J. C. Eriksson and S. Ljunggren, "Thermodynamic evaluation of the polydispersity of droplet microemulsions," Langmuir **11**(4), 1145–1153 (1995).
[43]S. A. Safran, "Fluctuations of spherical microemulsions," J. Chem. Phys. **78**(4), 2073–2076 (1983).
[44]P. D. I. Fletcher and J. F. Holzwarth, "Aggregation kinetics of oil-in-water microemulsion droplets stabilized by $C_{12}E_5$," J. Phys. Chem. **95**(6), 2550–2555 (1991).
[45]U. Olsson and P. Schurtenberger, "Structure, interactions, and diffusion in a ternary nonionic microemulsion near emulsification failure," Langmuir **9**(12), 3389–3394 (1993).
[46]P. D. I. Fletcher and D. N. Petsev, "A model for the temperature-dependent interactions in uncharged droplet microemulsions," J. Chem. Soc., Faraday Trans. **93**, 1383–1388 (1997).
[47]Y. Kawabata, H. Seto, M. Nagao, and T. Takeda, "Temperature- and pressure-dependences of shape fluctuations in a ternary microemulsion system," J. Neutron Res. **10**(3), 131–136 (2002).
[48]B. Kuttich, P. Falus, I. Grillo, and B. Stühn, "Form fluctuations of polymer loaded spherical microemulsions studied by neutron scattering and dielectric spectroscopy," J. Chem. Phys. **141**(8), 084903 (2014).